

Investigating the Effect of Separation Speed and Image Cross-Section Geometry on The Separation Force in DLP Method using FEP and PP Polymer Membranes

Siavash Moayedi Manizani¹, *, Jamal Zamani²,
Mohammad Salehi³, Mohammad Shayesteh⁴

Department of Mechanical Engineering,
University of KNTU, Iran

E-mail: Moayedi@Email.kntu.ac.ir, zamani@kntu.ac.ir,
m.salehi@Email.kntu.ac.ir, Shayesteh@Email.kntu.ac.ir

*Corresponding author

Received: 10 October 2022, Revised: 6 February 2023, Accepted: 21 February 2023

Abstract: One of the most challenging issues in DLP 3D printing is separation. Thus, the capability to employ a variety of polymer membranes can considerably aid in the development of the DLP technology. The primary purpose of this study is to thoroughly explore the characteristics influencing separation force and time on the FEP industrial membrane and the proposed PP membrane. Therefore, the impact of image cross section geometry and separation speed on separation force and separation time is investigated. As a consequence, changing the percentage of surface porosity has a negligible effect on the amount of separation force. According to the findings, reducing the cross-sectional area by 1.36% reduced the separation force by 6.5 times. Moreover, the outcomes are consistent with the mathematical model given. the separation force rose by 230% in the FEP membrane with an increase of 96 times of the speed, whereas the separation time decreased by 18.8 times. For the proposed PP membrane, as the speed increases, the separation force rate increases by 175% and the separation time falls by 29.6 times. The aforementioned findings show that the PP film may be used as a practical and affordable solution with quick separation that can reduce printing time when producing three-dimensional lattice pieces at varying speeds.

Keywords: Additive Manufacturing, Cross-section, Digital Light Processing, Photopolymerization, Separation Force, Separation Speed

Biographical notes: Siavash Moayedi Manizani, received his MSc in Mechanical Engineering from KNTU University, Tehran, Iran, in 2022. His current research field is additive manufacturing. Jamal Zamani received his PhD in Mechanical Engineering from Tarbiat Modares University, Tehran, Iran, in 2003. Mohammad Salehi, received his MSc in Mechanical Engineering from KNTU University, Tehran, Iran, in 2022. His current research field is additive manufacturing. Mohammad Shayesteh received his MSc in Mechanical Engineering from KNTU University, Tehran, Iran, in 2022. His current research field is additive manufacturing.

Research paper

COPYRIGHTS

© 2023 by the authors. Licensee Islamic Azad University Isfahan Branch. This article is an open access article distributed under the terms and conditions of the Creative Commons Attribution 4.0 International (CC BY 4.0)

<https://creativecommons.org/licenses/by/4.0/>



1 INTRODUCTION

Digital Light Processing (DLP) is one of the most precise and widely used technologies for producing 3D parts in additive manufacturing (DLP) [1]. A light beam with a wavelength of (355-410 nm) interacts with the photopolymer resin to form a bond between the resin monomers and eventually print the solid part in the digital light processing method [2]. This method can be applied in a variety of fields, including dentistry, tissue engineering, microfluidics, microneedle injection, and drug delivery [3-7]. Various systems have been created and designed for manufacturing 3D resin parts using several production processes. Due to the simultaneous development of plates or layers, the digital light processing approach is faster and more effective than the stereolithography method or the formation of points (pixel by pixel) [8]. The amount of force produced during separation by adhesion between the curing region and the container bed membrane might be considered as one of the method's limitations [9]. Numerous methods have been tried and tested to mitigate the separation force, including changing the separation mechanism [10], selecting materials for the container bed with adequate adhesive and elastic properties [11-15], utilizing grooved geometric patterns to reduce the contact cross-sectional [15], optimizing the layer-by-layer behavior model of the part surface and the container bed [12], [14], optimization of parameters such as image cross-sectional [10], separation speed and distance separation [14]. A few techniques have been proposed to separate printed layers, one of which is the flexible membrane [14]. A flexible membrane has been employed as a printing bed in this study. The printing platform and the underlying membrane of the container form an adhesion after each layer is formed as a result of the polymerization process. It produces a force called the separation force (Fig. 1). The impact of this force on a particular type of membrane, occasionally with diverse thicknesses, has been studied in the past [19].

According to these findings, raising the separation force can result in printing failure and decrease the membrane's lifespan [16-17]. The cross-sectional area of the image, the speed of separation, the type of membrane, the type of photopolymer resin, and the intensity of light are all parameters that influence this separation force. The amount of the layers' adhesion to the bottom plate and the required force to overcome this adhesion have been investigated in the experimental study associated with this article, utilizing the system designed and constructed using the digital light processing method. Additionally, to introduce the parameters affecting this force, such as the separation speed and the geometry of the cross section of the image, research was conducted on the introduction of a

polypropylene (PP) membrane and its comparison with the Fluorinated Ethylene Propylene (FEP) membrane, the most prevalent membrane used in DLP printers. As a result, the primary goal of recognizing and introducing polypropylene membrane is to develop more practical DLP 3D printers with a new flexible membrane, as well as to increase the availability of various membranes at a lower cost and with the same efficiency as the printing industry's common FEP membrane.

2 INTRODUCING THE SYSTEM

The system utilized in this study is a 3D printing system which uses the digital light processing method. This system was completely developed and created at the research lab of Khajeh Nasir Toosi University. It will hereafter be referred to as the Ultra system. The Ultra system's photopolymerization technique is able to print polymer pieces up to 80 mm x 65 mm x 45 mm in size. A transparent polymer sheet composed of acrylic (poly-methyl-methacrylate) is inserted under the membrane to calibrate the printing platform and prevent the membrane's elasticity in the container's bed.

A precise control and movement system is required in layer-by-layer additive manufacturing methods, such as digital light processing, to be able to determine and control the curing thickness of each layer. Using slicer software, the STL-format CAD models are converted to two-dimensional ultraviolet images, G-codes, and then sent to the optical unit system. When this ultraviolet light comes into contact with the photosensitive resin, it forms a chemical bond between the resin monomers and cures a layer between the printing platform and the bed. To build the next layer, it is important to modify the distance (in accordance with the layer's thickness) after each layer has been cured. This displacement of the printing plate is accompanied by the tensile tension between the printed part and the container bed. Different parameters, which will be covered in more detail later, affect the reduction of separation force ("Fig. 41").

3 MATERIALS AND EQUIPMENT

3.1. Resin and Container

The transparent flexible membrane is placed in the container bed by a mechanism built into the resin container itself. In this experiment, Transparent FEP and PP membranes with a 100 μ thickness were used. The membrane must be at least 240 mm x 180 mm in order to connect to the container's bed. Under the membrane, there is also a transparent acrylic sheet with a 4 mm thickness. Anycubic resin (Anycubic Company, USA), which has a viscosity of 522 MPa/s, a curing wavelength of 405 nm, and a tensile strength of 23.4 MPa, is the resin that is utilized.

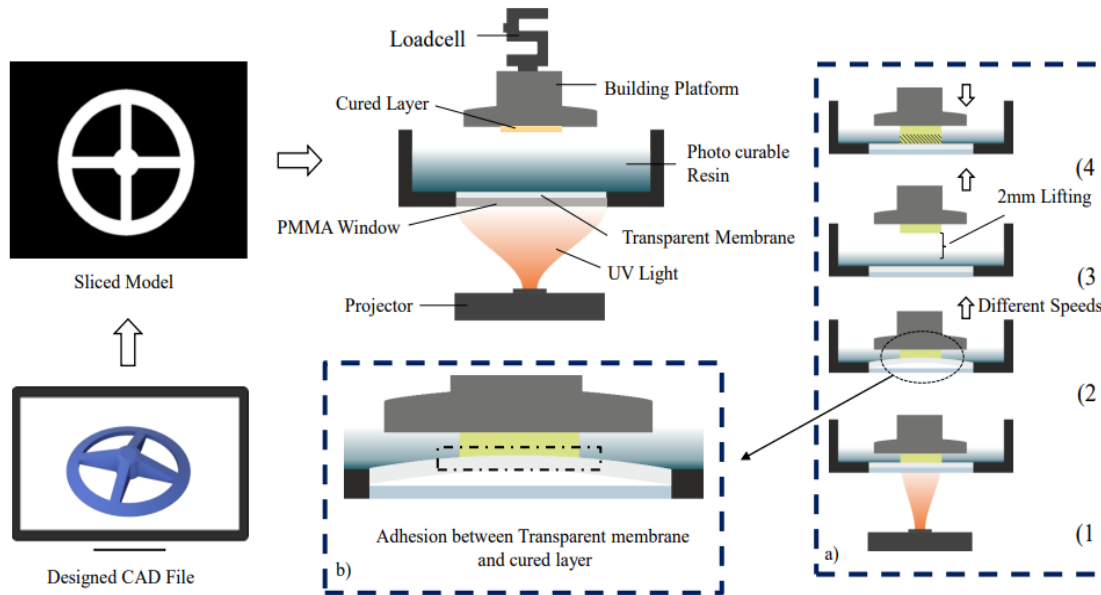


Fig. 1 The steps for 3D printing parts using digital processing, as well as how to separate each layer from the container's substrate membrane.

3.2. Optics and Light

This system incorporates a DLP projector with a resolution of 768 x 1024 pixels (XGA), a metal halide light source with a brightness of 3000 lumens. Digital micro-mirrors are typically mounted on a minuscule system in DLP projectors. The desired pixels can be viewed as the images of each layer when the light from the light source meets these micro-mirrors. The projector's light source shines directly below the container's bed. The maximum intensity of ultraviolet light in the unmediated state above the bed, is 8 mW/cm². Using ultraviolet light absorbers to lessen the projector's light intensity is a very effective way to manage the curing region and improve dimensional accuracy. The light intensity was tuned to 0.2 mW/cm² after going through the light absorbers [18]. The same research team designed and made these absorbers from polyester films.

3.3. Measuring Equipment

In this 3D printing system, a dynamometer sensor (SEWHACNM, Korea) with a maximum capability of measuring up to 50 newton of force is utilized online on the printing platform to check the separation force between the part and the flexible membrane. Additionally, a UV light measurement sensor (SPARKFUN, United States) was utilized to determine how much ultraviolet light was emanating from the source.

4 TEST METHOD AND RESULTS

One of the key elements of the digital light processing method is separation force. This force is influenced by a number of variables, including the type of separation mechanism, the type of container bed, and the system input parameters. The majority of studies have addressed the issue of reducing the separation force on lattice structures in a container with a fixed separation method in their articles, in addition to the previously mentioned variables. However, in this article, we also experimentally studied the aforementioned variables on two distinct types of polymer membranes to see how they affected the separation force. Additionally, a theoretical model has also been evaluated to predict the suction force of the fluid after separation with the circular cross-sectional area.

4.1. Test Results Related to The Theory of Fluid Adhesion Force and Circular Solid Cross Section

After being exposed to UV light, the polymerization process in light-sensitive resin molecules causes a layer to cure in bottom-up photopolymerization procedures ("Fig. 2a"). It has separated the created polymer from the constrained surfaces by moving the printing platform upward, which is separated from the surface of the polymer membrane with force and time consumption. In the meantime, liquid resin fills the space between the printing sheet and the container bed as a result of the pressure difference that is formed ("Fig. 2c"). When determining fluid adhesion force, variables like resin

viscosity, separation speed, and layer cross-sectional geometry are crucial. The suction force during the production of a symmetrical part is predicted by the model that is presently being used. The model has the following information: a solid cylindrical component

with radius R, a solid bottom surface, and a constant, time-invariant resin viscosity. According to “Fig. 2d”, the tensile force F is generated in the direction of the axis' motion when the printing platform is moving at a specific speed V.

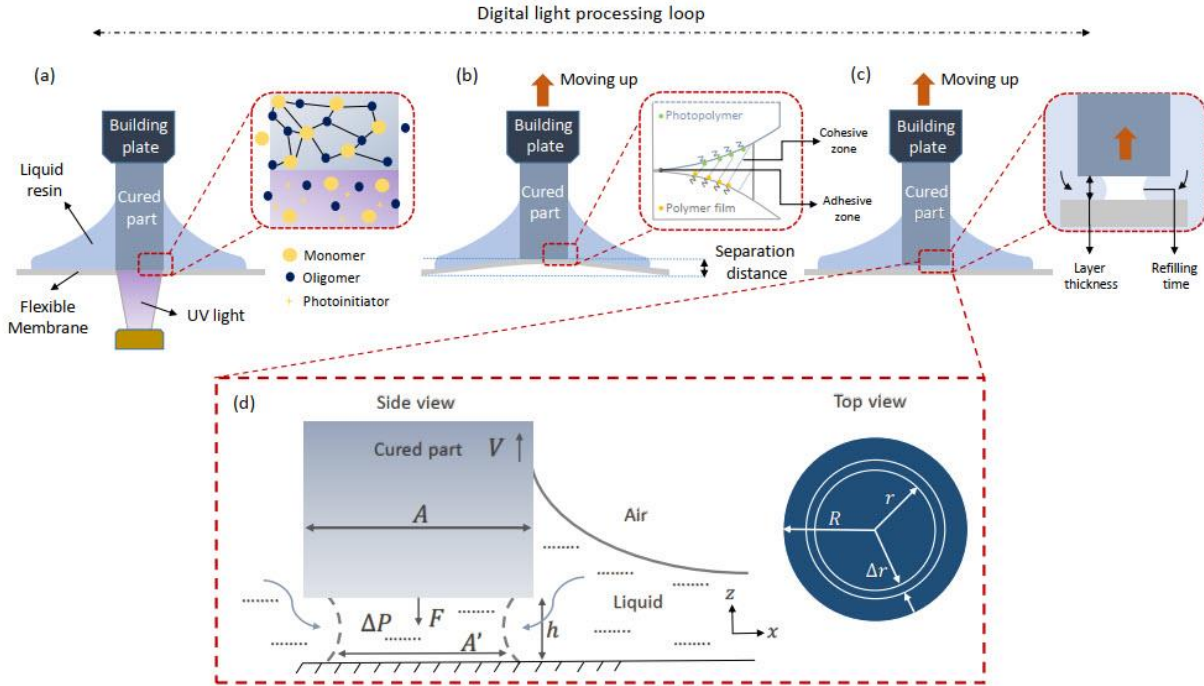


Fig. 2 Steps of making a polymer layer in DLP method with the bottom-up construction mechanism: (a): UV light irradiation and the initiate of the polymerization process between the resin molecules, (b): movement of the printing plate and separation of the cured layer from the polymer membrane, (c): continue to move the printing plate after separation to create resin flow under the part, and (d): Two-dimensional model of fluid separation force with circular solid cross-section [16].

Additionally, A and h represent, respectively, the height between the cured layer and the container bed and the area of the dried cross-section. This article aims to accurately calculate the adhesion force resulting from the fluid inside a container using a mathematical model presented in the references. With the help of the Navier-Stokes velocity equation and the flow rate formula, the applied force of the fluid movement can be evaluated.

$$u = \frac{1}{2\mu} \frac{dp}{dr} (z^2 - z \times h) \quad (1)$$

The quantity of force is computed from the equality of the suction channel's intake and output flow rates, and the following relationship is established:

$$V \cdot \pi r^2 = \int_0^h u \, dA \quad (2)$$

$$= 2\pi r \int_0^h u \, dz$$

The amount of suction pressure is determined based on movement speed by evaluating the integral of “Eq. (2)”.

The pressure equation's constant quantity and the final suction pressure are measured using the boundary conditions (P = 0 and R = r):

$$P = -\frac{3\mu V}{h^3} \cdot r^2 + \frac{3\mu V}{h^3} \cdot R^2 \quad (3)$$

As a result, the force generated by the part's movement is calculated using the area's surface pressure.

$$F = \int_0^R 2\pi r P \, dr = \frac{3\pi \cdot \mu V}{2 \cdot h^3} \cdot R^4 \quad (4)$$

Fluid adhesion force F with circle radius R and separation height h is nonlinear according to the model. Additionally, there is a direct and linear relationship between the adhesion force and the rate of separation speed. This model states that the adhesion force decreases with reducing separation speed, increasing

distance between two surfaces, and decreasing geometry of the cross section. Therefore, in the discussion of minimizing adhesion force, experimental tests have been designed as described below to corroborate this finding:

4.2. Experiments Related to Image Cross Section Geometry and Separation Force

Two methods of measuring the area and perimeter of each layer of two-dimensional images on the FEP membrane with a thickness of 100 micrometre were investigated in order to confirm the impact of the cross section's geometry. In this segment, the layer separation force is studied first using lattice cylinders with porosity percentages of 35.5%, 27.57%, and 68.62% and a 20 mm diameter cylinder with a cross-sectional area of 314 mm² ("Table 1"). The study was conducted using a separation speed of 50 mm/h. However, the relationship between the separation force and the porosity percentage is quite complicated.

Table 1 Separation force and time in different cross-sections with the same diameter

CAD models				
Part's Name	L1	L2	L3	L4
Cross-sectional area (mm ²)	117.18	134.17	202.53	314
Porosity percentage (%)	62.68	57.27	35.50	0
Separation Force (N)	1.78	1.79	1.68	2.25
Separation Time (s)	1.14	1.19	1.25	1.32

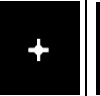
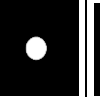
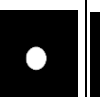
The number of bright pixels in each layer and the largest diameter of the perimeter where the images are placed are indicated by the area and perimeter of the surfaces of each layer, respectively. Three pyramid parts with various porosity percentages were used to test the impact of the part's design on the separation force and to look into how the environment affected it. In this experiment, the influence of surface perimeter on separation force in 4 layers was explored in addition to comparing the surface areas in layers 1, 30, 60, and 90. In a specific layer, the maximum perimeter diameter is the same for all three parts (G1, G2, and Full). In this experiment, in addition to comparing the surface area in layers 1, 30, 60, and 90, the influence of surface perimeter on separation force in 4 layers was explored. The maximum perimeter diameter is supposed to be the same as the specific layer's three components (G1, G2, and Full) ("Table 2").

4.3. The Effect of Separation Speed and Membrane Type on The Separation Force

A fixed cylindrical part with dimensions of 20 mm x 1.5 mm, a slice thickness of 0.05 mm for each layer, and

speeds of 5, 10, 20, 50, 80, 150, 450 mm/min, printing and separation force data were recorded online by the dynamometer sensor in order to observe the effect of speed on the separation force.

Table 2 Comparison of area and perimeter of solid pyramidal and lattice parts in 4 special layers

Designed model	Slice1	Slice30	Slice60	Slice90	Part
maximum diameter (mm)	25	18.25	10.75	6.5	Part
					G1
Area (mm ²)	256.76	73.04	42.93	8.3	
					G2
Area (mm ²)	252.76	233.51	90.76	8.3	
					Full
Area (mm ²)	490.87	261.59	90.76	8.3	

After the formation of a polymer layer between the printing platform and the container bed, the adhesive force is formed between these two surfaces. These two surfaces must be separated up to a specified height in order to reflow the liquid resin there and create the subsequent layer. In accord with "Table 3", the separation force and separation time in two polymer membranes, FEP and PP, have been compared in the container bed by changing the separation speed in each layer.

One of the most effective variables for accelerating the printing speed of parts and drastically reducing printing time is separation speed. The speed boost in the digital light processing method is constrained by the adhesion between the two surfaces of the printing plate and the bed. As a consequence of this, to overcome this adhesion force, it is necessary to spend time and reduce speed.

Table 3 Comparing force and separation time in the two mentioned membranes at different speeds

Separation Time (s)		Separation Force (N)		Speed (mm/h)
FEP	PP	FEP	PP	
1.17	1.81	8.3	7.9	450
1.50	1.96	6.1	5.1	150
1.95	2.72	3.1	2.8	80
2.32	3.01	2.2	1.6	50
2.93	4.15	1.4	0.9	20
3.41	4.25	1.1	0.8	10
3.85	4.95	0.8	0.5	5

Additionally, the definitive separation of the layer and the reflow of the liquid resin depend greatly on the separation height or distance of the printing platform. This parameter has not been looked into in this article. The results of the experimental testing are shown in the following sections. It is evident from these results that it is crucial to understand the precise amount of adhesion force for various membranes.

5 DISCUSSION AND EXAMINATION OF THE RESULTS

The aforementioned cases were looked into, in order to determine the quantity of adhesion force and its relationship to other important factors in the fabrication of parts. "Table 4" lists the constant printing parameters for the Ultra 3D printing system. The results of experimental tests are next examined, and these results are then discussed.

5.1. Effect of Image Cross-Section on Separation Force

Investigating the effect of cross-sectional area of the image was evaluated with two approaches, area and

environment. Figure 3 illustrates how decreasing the area of the image while maintaining the same diameter of the outer circle has no tangible effect on the separation force, which is stated to be approximately the same for the various porosity percentages.

Table 4 Printing parameters in ULTRA DLP 3D printer

Print parameters	value
Resin volume	336 cm ³
Aspect ratio of the projector	4:3
UV intensity	0.2 mW/cm ²
Exposure Time	6.2 s
Average print speed	10 mm/h

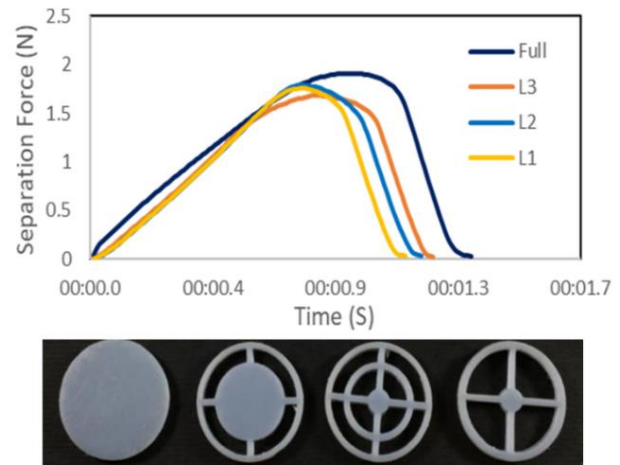


Fig. 3 Comparing the porosity percentage of each layer on the force and time of separation and the view of the printed parts.

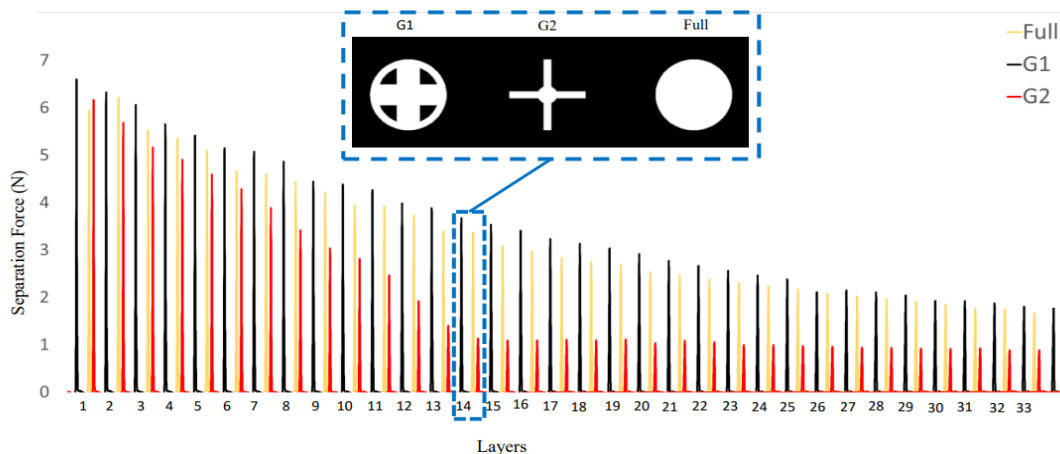


Fig. 4 Separation force in three pyramid-shaped parts with varying percentages of porosity in each layer and parts printed with The Ultra 3D printer.

Additionally, it was found that as the porosity of the layers' cross-section increased, so did the printing and separation times. Three pyramids (G1, G2, and Full) were printed with various cross-sectional areas in order to investigate the behavior of separation force at different cross-sectional areas and to demonstrate the efficiency of the PP membrane. Also, the changes of the cross-sectional image in layers 1, 30, 60, and 90 are depicted according to "Table 2". In this experiment, the peripheral diameter of the images was decreased by increasing the number of layers. For instance, in layer 30, all three pieces have the same peripheral diameter of 18.25, yet each layer's area is distinct from one another. The mentioned three parts' behavior in the 33 primary layers is seen in "Fig. 4". The general downward trend of this graph is brought on by the cross-sectional area decrease and the pyramidal form of the component sections. As can be observed, despite the change in the parts' overall shape and the porosity percentage for each slice, the trend and behavior of the separation force for the full and G1 parts are very similar. In the case of the G2 parts, the separation force is significantly reduced by reducing the perimeter of each section compared to the sections of the other two parts.

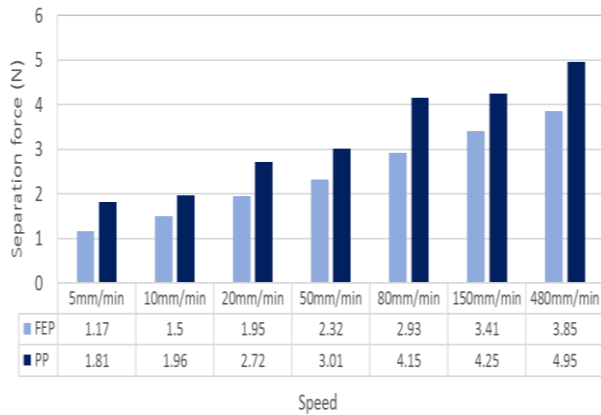


Fig. 5 Comparing the separation force of two polymer membranes with different separation speeds.

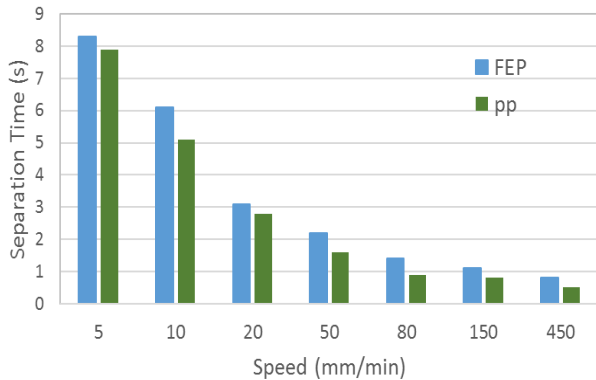


Fig. 6 Separation time of two polymer membranes at different separation speeds in one layer.

5.2. The Effect of Separation Speed on Separation Force

In order to investigate the effect of speed on the separation force in this research, for the two mentioned membranes, a cylindrical piece with a diameter of 20 mm was printed whereas maintaining the printing parameters such as resin type, UV intensity and separation height of 2 mm at speeds of 5, 10, 20, 50, 80, 150 and 450 mm/hour ("Fig. 5"). According to "Fig. 6", both membranes first experience an increase in separation force along with an increase in separation speed.

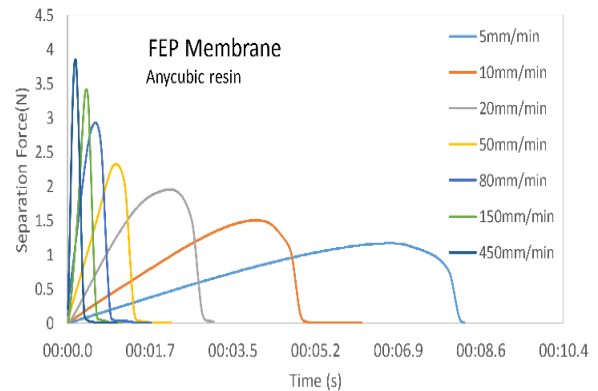


Fig. 7 Separation force vs separation time diagram for FEP polymer membranes with varying separation speeds.

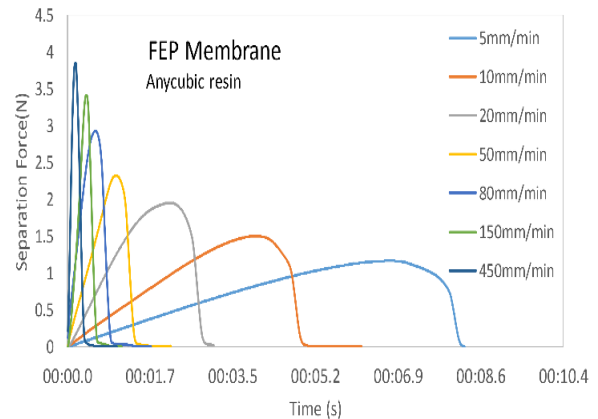


Fig. 8 Separation force vs separation time diagram for FEP polymer membranes with varying separation speeds.

Whereas in general, the use of FEP membrane leads to the production of less separation force. According to the separation force diagram at a speed of 50 mm/hour, this force is 2.32 newton for the FEP membrane and 3.01 newton for the PP membrane, demonstrating a minor variation in separation force between these two membranes. Additionally, the fact that FEP membrane's percentage rise in separation force is 230% while PP membrane's is 175% indicates that PP membrane's rate

of force growth is slower than that of FEP membrane. Other data obtained from “Fig. 7” clearly demonstrates that the separation times of each layer in both membranes decrease with increasing speed, that the separation times in the PP membrane are very similar to those in the FEP membrane, and that the separation times decrease by 96 times with an increase in speed. It causes a reduction of 8.18 and 6.29 times, respectively, in PP and FEP membranes. The following is an online separation force diagram for a particular layer of circular cross-section with a diameter of 20 mm. The graphs below illustrate the amount of separation force for PP and FEP membranes at various speeds. According to “Fig. 7” and “Fig. 8”, increasing the separation speed increases the separation force while decreasing the separation time of the layer from the membrane surface.

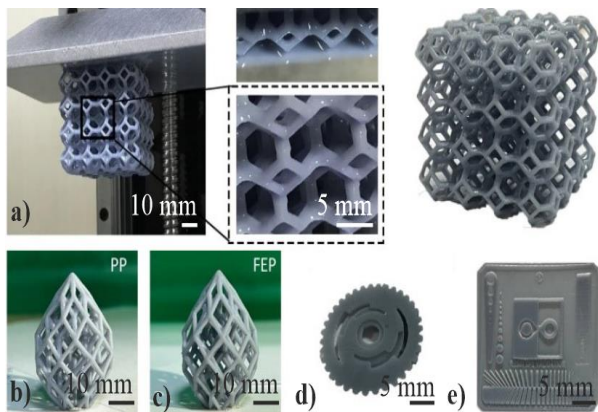


Fig. 9 Lattice and complex parts printed by Altra DLP 3D printer with PP polymer membrane: (a): Lattice cubic part, (b): Lattice flower part using PP membrane, (c): Flower lattice part using FEP membrane, (d): Complex gear, and (e): High detail calibration part.

6 CONCLUSIONS

The effects of the separation force in the additive manufacturing process using the optical digital processing method and the flexible membrane mechanism were explored in this paper. This force is dependent on factors such as resin viscosity, separation speed, cross-sectional area, and separation height, according to theoretical relationships. The experimental results show that the separation speed and the geometry of the image section surface have a direct effect on the separation force, and is the most optimal arrangement for the occurrence of the lowest separation force, to reduce the image area of the cross section and the separation speed. In addition, with a 96-fold increase in speed, the separation force increases by 230%, while the separation time decreases by 8.18 times. The data above are also true for the PP membrane, and as the speed

increases, the separation force rate increases by 175% and the separation time drops by 29.6 times. This indicates that the PP membrane may be utilized as a rapid separation membrane to save printing time, and it can be inferred that this membrane is a cost-effective and viable option for producing three-dimensional parts with different speeds. Some of the parts made with this membrane are represented in “Fig. 9”.

REFERENCES

- [1] Ge, Q., Li, Z., Wang, Z., Kowsari, K., Zhang, W., He, X., and et al, Projection Micro Stereolithography Based 3d Printing and Its Applications, International Journal of Extreme Manufacturing, Vol. 2, No. 2, 2020, pp. 022004, DOI: <https://doi.org/10.1088/2631-7990/ab8d9a>.
- [2] Zhang, B., Kowsari, K., Serjouei, A., Dunn, M. L., and Ge, Q., Reprocessable Thermosets for Sustainable Three-Dimensional Printing, Nature communications, Vol. 9, No. 1, 2018, pp. 1831, DOI: <https://doi.org/10.1038/s41467-018-04292-8>
- [3] Choo, S., Jin, S., and Jung, J., Fabricating High-Resolution and High-Dimensional Microneedle Mold Through the Resolution Improvement of Stereolithography 3D printing, Pharmaceutics, Vol. 14, No. 4, 2022, pp. 766, DOI: <https://doi.org/10.3390/pharmaceutics14040766>.
- [4] Hazeveld, A., Slater, J. J. H., and Ren, Y., Accuracy and Reproducibility of Dental Replica Models Reconstructed by Different Rapid Prototyping Techniques, American Journal of Orthodontics and Dentofacial Orthopedics, Vol. 145, No. 1, 2014, pp. 108-15, DOI: <https://doi.org/10.1016/j.ajodo.2013.05.011>.
- [5] Kadry, H., Wadnap, S., Xu, C., and Ahsan, F., Digital Light Processing (DLP) 3D-Printing Technology and Photoreactive Polymers in Fabrication of Modified-Release Tablets, European Journal of Pharmaceutical Sciences, Vol. 135, 2019, pp. 60-7, DOI: <https://doi.org/10.1016/j.ejps.2019.05.008>.
- [6] Razavi Bazaz, S., Rouhi, O., Raoufi, M. A., Ejeian, F., Asadnia, M., Jin, D., and et al., 3D Printing of Inertial Microfluidic Devices, Scientific Reports, Vol. 2, No. 1, 2020, pp. 5929, DOI: <https://doi.org/10.1038/s41598-020-62569-9>.
- [7] Skoog, S. A., Goering, P. L., and Narayan, R. J. Stereolithography in Tissue Engineering, Journal of Materials Science: Materials in Medicine, Vol. 25, 2014, pp. 845-56, DOI: <https://doi.org/10.1007/s10856-013-5107-y>.
- [8] Truxova, V., Safka, J., Seidl, M., Kovalenko, I., Volesky, L., and Ackermann, M., Ceramic 3D Printing: Comparison of SLA and DLP Technologies, MM Sci. J., Vol. 2020, pp. 3905-11, DOI: http://dx.doi.org/10.17973/MMSJ.2020_06_2020006.
- [9] Stansbury, J. W., Idacavage, M. J., 3D Printing With Polymers: Challenges Among Expanding Options and

- Opportunities, *Dental Materials*, Vol. 32, No. 1, 2016, pp. 54-64, DOI: <https://doi.org/10.1016/j.dental.2015.09.018>.
- [10] Lin, Y. S., Yang, C. J., Spring Assisting Mechanism for Enhancing The Separation Performance of Digital Light Process 3D Printers, *IEEE Access*, Vol. 7, 2019, pp. 71718-29, DOI: <https://doi.org/10.1109/ACCESS.2019.2920004>.
- [11] Huang, Y. M., Jiang, C. P., On-Line Force Monitoring of Platform Ascending Rapid Prototyping System, *Journal of Materials Processing Technology*, Vol. 159, No. 2, 2005, pp. 257-64, DOI: <https://doi.org/10.1016/j.jmatprotec.2004.05.015>.
- [12] Liravi, F., Das, S., Zhou, C., Editors, Separation Force Analysis Based on Cohesive Delamination Model for Bottom-Up Stereolithography Using Finite Element Analysis, 2014 International Solid Freeform Fabrication Symposium, University of Texas at Austin, 2014.
- [13] Tijjing, L. D., Dizon, J. R. C., Ibrahim, I., Nisay, A. R. N., Shon, H. K., and Advincula, R. C., 3D Printing for Membrane Separation, Desalination and Water Treatment, *Applied Materials Today*, Vol.18, 2020, 100486, DOI: <https://doi.org/10.1016/j.apmt.2019.100486>.
- [14] Wu, X., Xu, C., and Zhang, Z., Flexible Film Separation Analysis of LCD Based Mask Stereolithography, *Journal of Materials Processing Technology*, Vol. 288, 2021, pp. 116916, DOI: <https://doi.org/10.1016/j.jmatprotec.2020.116916>.
- [15] Ye, H., Venketeswaran, A., Das, S., and Zhou, C., Investigation of Separation Force for Constrained-Surface Stereolithography Process From Mechanics Perspective, *Rapid Prototyping Journal*, Vol. 23, No. 4, 2017, pp. 696-710, DOI: <https://doi.org/10.1108/RPJ-06-2016-0091>.
- [16] Pan, Y., He, H., Xu, J., and Feinerman, A., Study of Separation Force in Constrained Surface Projection Stereolithography, *Rapid Prototyping Journal*, Vol. 23, No. 2, 2017, pp. 353-61, DOI: <http://dx.doi.org/10.1108/RPJ-12-2015-0188>.
- [17] Wu, J., Guo, J., Linghu, C., Lu, Y., Song, J., Xie, T., and et al., Rapid Digital Light 3D Printing Enabled By a Soft and Deformable Hydrogel Separation interface, *Nature Communications*, Vol. 12, No. 1, 2021, pp. 6070, DOI: <https://doi.org/10.1038/s41467-021-26386-6>.
- [18] Springer, S., UV and Visible Light Filtering Window Films, *WAAC Newsletter*, Vol. 30, No. 2, 2008, pp. 16-23, Electronic Publications.
- [19] ETEC 2022, 3D Printers|Desktop, Professional and Industrial|EnvisionTEC, [online] Available at: <https://envisiontec.com/aria-desktop-3d-printer/> 2022.